The β-lactam Ticarcillin *is a Staphylococcus aureus* UDP-N-acetylglucosamine 2-epimerase binder.

Erika Chang de Azevedo[1] and Alessandro S. Nascimento[1*].

[1]. Instituto de Física de São Carlos, Universidade de São Paulo. Av. Trabalhador SaoCarlense, 400. Parque Arnold Schmidit. São Carlos, SP, Brazil. 13566-590.

[*] Corresponding author. E-mail: asnascimento@ifsc.usp.br. Phone: +55-16-3373-8709.

Abstract

Infectious diseases account for 25% of the causes of death worldwide and this rate is expected to increase with the increasing rate of antibiotic resistance observed for many pathogens. Among the bacterial pathogens usually found in healthcare associated infections, *Escherichia coli* and *Staphylococcus aureus* are the most prevalent pathogens and, for the former, about 50% of the isolates are found to be methicillin resistant. Given the limited number of targets/pathways observed for the mechanism of action for the existing antibiotics, the discovery of newer targets and their evaluation becomes an urgent and necessary task. Here we describe the structure-based identification of ticarcillin as a weak binder of the UDP-N-acetylglucosamine 2-epimerase (MnaA) from *S. aureus*. After a docking-based screening of existing drugs, ticarcillin was identified as a ligand in isothermal analysis of differential scanning fluorimetry data. An equilibrium molecular dynamics simulation confirmed the docking binding mode as a stable pose, with large contributions to the binding energy coming from interactions between Arg206 and Arg207 and the carboxylate groups in ticarcillin.

32 # 1. Introduction

33

34 The Gram-positive bacteria *Staphylococcus aureus* is listed by the Center of Disease
35 Control (CDC) at USA among those bacteria that represent a serious threat to humans due to
36 their high rates of observed antibiotic resistance [1]. The number of infections caused by
37 methicillin-resistant *S. aureus* (MRSA) strains per year reaches 80,000, resulting in a about
38 11,000 deaths [1]. Also, according to the survey taken by the National Healthcare Safety
39 Network at the Centers for Disease Control and Prevention, USA, *S. aureus* was ranked as the
40 second most frequent organism causing healthcare-associated infection, after *Escherichia*
41 *coli*, and was responsible for about 12% of the reported infections [2].

42 The same report also brings an interesting, though worrying, data. According to the
43 data collected from 2011-2014, about 50-52% of the *S. aureus* clinical isolates from central
44 line-associate bloodstream infections were reported to be resistant to methicillin. From
45 isolates from catheter-associated urinary tract infections, about 52-57% were reported to be
46 methicillin-resistant. From isolates from ventilator-associated pneumonia and from surgical
47 site infections, 42-44% were reported to be resistant [2]. The data from 2009-2010 also
48 indicates that the rates in resistance for *S. aureus* follows a worrisome trend, with about 50%
49 of the Staphylococcal healthcare-associated infections being caused by a resistant strain [3].

50 The estimated number of people with important infections caused by antibiotic
51 resistant bacteria reached 2,000,000 in 2013, with 23,000 deaths directly caused by these
52 infections [1]. In Europe, about 25,000 deaths were related to antibiotic resistant bacteria in
53 2007 by the European Center of Disease Prevention and Control [4]. The estimated number
54 of deaths per year caused by antibiotic resistance globally reaches 700,000, highlighting the

55 burden caused by resistant bacteria [5]. In addition, Thorpe and coworkers estimated that
56 antibiotic resistance results in additional $1,383 to the cost of the treatment per patient,
57 resulting in an annual cost of 2.2 billion dollars in the US [6].

58 The bacterial cell envelope, first line of defense for bacteria against changes in the
59 environment, is also the target of the first-choice antibiotic for treating many *S. aureus*
60 infections. The beta-lactam antibiotics act by binding and inhibiting the penicillin-binding
61 proteins (PBPs) [7], impairing the transpeptidase activity and resulting in the inhibition of the
62 peptidoglycan synthesis. The cell envelope in Gram-positive bacteria such as *S. aureus*, is also
63 decorated with the wall teichoic acid (WTA) [8], which are polymers containing 40-60 polyol
64 repeats and can account for up to 60% of the cell wall mass [8]. The association between beta-
65 lactam antibiotic resistance and the composition of the WTA has been shown, although the
66 precise mechanisms underlying this association are not completely clear yet. Brown and
67 coworkers showed that the deletion of the glycosyltransferase (GT) TarS, responsible for the
68 decoration of the WTA with β-O-GlcNAc, can re-sensitize MRSA strains to beta-lactam
69 antibiotics [9]. Additionally, it has been shown that some PBP can interact with the WTA [10],
70 again suggesting some cross-talk between the WTA and the mechanism of action of the beta-
71 lactam antibiotics.

72 WTA itself is a very interesting target for the development of new antibiotic
73 candidates. Tarocins and tunicamycin, for example, were shown to act on the synthesis of the
74 WTA by inhibiting the first enzyme of the biosynthesis pathways, TarO [11], with bactericidal
75 effects on resistant bacteria and also with synergistic effects with beta-lactam antibiotics.
76 Tunicamycin, not only inhibits TarO but also inhibits MnaA, an UDP-N-acetylglucosamine 2-
77 epimerase that provides the appropriate concentrations of UDP-GlcNAc and UDP-ManNAc
78 for the further steps of the biosynthetic pathway [12,13].

As highlighted by Walsh and Wencewicz, the antibiotics under use currently are limited to only five major validated targets/pathways [14]. So, given the scarcity of targets and the relevance of the cell wall decoration for *S. aureus*, we report here the structure-based screening for new MnaA binders using a catalogue of existing drugs in a repurposing strategy [15]. After molecular docking and careful visual inspection, we identified fifteen ligand candidates. Further experimental evaluation with quantitative DSF (qDSF) revealed ticarcillin, a β-lactam, as a weak binder for *S. aureus* MnaA (SaMnaA). An equilibrium molecular dynamics simulation confirmed a stable binding pose over 600 ns with strong interactions between ticarcillin carboxylate groups and SaMnaA R206 and R207 residues.

2. Materials and Methods

2.1 Molecular Docking and Ligand Selection

The molecular model used for docking calculations was based on the crystal structure for *S. aureus* MnaA, PDB Id 5ENZ [13], with the same structure preparation procedure as previously described [16]. Briefly, the server H^{++} [17] was used to define the protonation states of residues and hydrogen atoms were added accordingly. The atom types and charges were defined according to AMBER FF14SB [18]. In this model, an UDP molecule was considered as a part of the 'receptor'. The atomic charges were computed using a RESP fitting procedure after initial calculations using Hartree-Fock method with 6-31G* basis, as available in Gaussian 09 [19]. The substrate UDP-GlcNAc was prepared using the same method and considered as the 'reference ligand' during the docking calculations. The ZINC Drug Database (ZDD) was used for the screening. The MOL2 files were used as provided by the database using the default ZINC methods for ligand preparation [20]. The docking calculations were set

104 up using LiBELa, a ligand- and receptor-based docking software developed in our group
105 [21], using a pre-computed DelPhi [22,23] electrostatic potential for modeling the polar
106 interactions and a 6-12 Lennard Jones potential to model van der Waals interactions [24]. The
107 docking results were analyzed using the ViewDock tool available in UCSF Chimera [25] and
108 promising candidates were selected based on the visual inspection of favorable interactions
109 involving the ligand and the enzyme.

110

111 ## 2.2 SaMnaA expression and purification

112

113 *S. aureus* MnaA was cloned from a S. aureus SA16 gDNA sample kindly provided by Prof.
114 Dr. Ilana Camargo. The SaMnaA gene was amplified using the primers forward 5'-
115 CAGGGCGCCATGATGAAAAAGATTATGACCATATTTG-3' and reverse 5'-GACCCGACGCGGTTA
116 TCAGAAATCGCTTGGTTTT-3'. The amplified gene was inserted in the pET-Trx1A vector using
117 a strategy described elsewhere [26]. *E. coli* Rosetta (DE3) cells were transformed with the
118 resulting plasmid and used for protein expression. A starting culture was grown overnight in
119 LB medium supplemented with containing 50 μg/ml kanamycin. Afterward, the starting
120 culture was used to inoculate LB medium containing 50 μg/ml kanamycin. The cells were
121 incubated in a shaker at 18°C and, after reaching an Optical density of 0.8 at 600 nm, the
122 protein expression was induced with 0.1 mM IPTG. After 16 hours at 18°C, the cells were
123 harvested by centrifugation at 7800 x g for 30 min and disrupted by sonication in lysis buffer
124 containing 50 mM NaH_2PO_4, pH 8.0, 300 mM NaCl, 10 mM imidazole, 1 mM PMSF, 1 mg/mL
125 lysozyme. The soluble proteins were isolated from the cell debris by centrifugation at 18,000
126 x g for 30 min at 4°C and SaMnaA was purified by IMAC. Briefly, the soluble fraction was
127 incubated with 5 ml of the Ni resin equilibrated with washing buffer containing 50 mM
128 NaH_2PO_4, pH 8.0, 300 mM NaCl, 20 mM imidazole, 10% glycerol. After extensive washing,

129 MnaA was eluted in the same buffer supplemented with 500 mM imidazole. After dialysis to
130 remove the imidazole, and concentration up to about 2 mg/ml and incubated with a Tobacco
131 Etch Virus (TEV) protease for 16 hours at 4°C, to remove the fusion protein. A second IMAC
132 step was carried out to remove the His-tagged fusion protein thioredoxin. For crystallization
133 trials, an additional purification step was carried out with size exclusion chromatography
134 using a Superdex 75 column.
135
136 ## 2.3 Differential Scanning Fluorimetry (DSF)
137
138
139 Fourteen ligands were initially selected from docking calculations and were screened for
140 their ability to bind to *S. aureus* MnaA *in vitro* using a DSF assay. Briefly, SaMnaA at 2μM was
141 incubated with each ligand at a concentration of 6 μM (3:1 ratio) for 30 minutes. Afterwards,
142 the complex was incubated with SYPRO Orange dye (ThermoFisher) for DSF experiment using
143 a Bio-Rad CFX96 real-time PCR Detection System equipment using a temperature range of 25-
144 95 °C with a heating rate of 1°C every 30 seconds. The obtained data was adjusted according
145 to the unfolding model proposed by Bai and coworkers [27], that relates the measured
146 fluorescence intensity *Y* to the temperature *T* [27]:
147
148 $$Y(T) = \left[\frac{1}{1+K_U}(m_F T + b_F)\right] + \left[\frac{K_U}{1+K_U}(m_U T + b_U)\right] \quad (1)$$
149 where
150 $$K_U = e^{\frac{-\Delta G}{RT}} \quad (2)$$
151 and
152 $$\Delta G = \Delta H\left(1 - \frac{T}{T_m}\right) - \Delta C_P\left(T_m - T + T\ln\left[\frac{T}{T_m}\right]\right) \quad (3)$$
153

154 As previously described, the two terms in first equation account for the contributions of the
155 folded and unfolded protein, m_F/m_U and b_F/b_U account for the dependence of the dye when
156 the protein is folded/unfolded, thus incorporating the baselines and slopes, while K_U gives the
157 unfolded/folded equilibrium constant. T_m values were extracted from this initial fitting to the
158 DSF data, using ΔC_P as constant at 3.22 kcal/(mol.K), as estimated by the ScooP server [28],
159 and used to evaluate actual binders among the ligands selected from docking calculations.

160 For affinity constant calculations, the same protocol was used, varying the ligand
161 concentration from 0 to 2,000 μM. The thermal unfolding data was adjusted in the model
162 proposed by Bai and coworkers [27]. In this model, the fraction of unfolded protein f_U is given
163 as:

164 $$f_U = \frac{[U]}{[U]+[F]+[FL]} \quad (4)$$

165 Where [U] is the concentration of the unfolded protein, [L] is the free ligand concentration,
166 [F] and [FL] are the concentration of the folded in unbound and folded and bound protein,
167 respectively. The model assumes that only the folded species bind the ligand in the following
168 equilibrium:

169 $$[U] + [L] \underset{K_U}{\leftrightarrow} [F] + [L] \underset{K_d}{\leftrightarrow} [FL] \quad (5)$$

170 With

171 $$[P] = [F] + [U] + [FL] \quad (6)$$

172 $$[L]_T = [L] + [FL] \quad (7)$$

173 $$K_U = {[U]}/{[F]} \quad (8)$$

174 $$K_d = \frac{[F][L]}{[FL]} \quad (9)$$

175 Using equations 6-9, equation 4 can be rewritten as:

176 $$f_U = \frac{1}{1+[(1/K_U)\times(1+[L]/K_d)]} \quad (10)$$

177 After redefining the free ligand concentration [L] as a function of the total ligand
178 concentration $[L]_T$, f_U can be analyzed in terms of only two parameters, K_U and K_d, since $[L]_T$
179 and [P] are known [27]. All the data analysis was done using `DSF_fitting.py` python
180 script as described by Bai and coworkers [27]. All the tested compounds were purchased from
181 Merck-Sigma.

182

183 Molecular Dynamics Simulations

184

185 The docking pose found for Ticarcillin bound to *S. aureus* MnaA was used for
186 equilibrium MD simulations. Here, the same receptor preparation described was used. For
187 the ligand, RESP charges were computed after electrostatic potential calculation using HF/6-
188 31G*, using the same protocol as used for UDP and UDP-GlcNAc. Ligand atom types were
189 attributed according to GAFF2 [29]. The complex, containing MnaA and ticarcillin was
190 immersed in OPC solvation box with 150 mM NaCl and neutralized using tLeap. The system
191 was used for energy minimization, heating and equilibration using the same protocol as
192 previously described [16]. After, 5,000 minimization steps, the system was heated to 300 K in
193 50 ps using an NVT ensemble simulation, followed by 50 ps of an NPT simulation to equilibrate
194 the system density. For these preliminary equilibration steps, harmonic restraints were kept
195 in the initial coordinates of the ligands and the protein with an spring constant of 2.0
196 kcal/(mol.Å^2). Finally, 500 ps of NPT simulation was carried out for final equilibration,
197 followed a 600 ns productive simulation (NPT). For the final equilibration and productive
198 simulation, a weak positional restraint was kept at all α carbon atoms to avoid enzyme
199 opening with an spring constant of 1.0 kcal/(mol.Å^2). All the MD simulations were run with

200 SANDER, PMEMD and PMEMD.CUDA programs from the AMBER 20 package [30–33]. The MD
201 trajectory was analyzed using AMBERENERGY++ [34], a locally written program to compute
202 interaction energies, VMD [35], Chimera [25] and CPPTRAJ [36].
203

204 # Results
205

206 Given the relevance of *MnaA* in the synthesis of the WTA and the antibiotic relevance,
207 we used a structure-guided screening of compounds that could inhibit the enzymatic activity.
208 For this purpose, we used the ZINC Drug Database (ZDD), a catalogue of almost 3,000
209 purchasable drugs that were approved for use in humans in different countries [20]. The
210 rationale here involved the identification of binders that are already proved to be non-toxic
211 and with a tolerable pharmacokinetic profile. In a typical drug discovery pipeline, the
212 compounds could be further improved to improve its properties, including the affinity for the
213 target. In this context, the identification of a binder in the narrow chemical space would be a
214 challenge *per se*.
215 After visual inspection of the docking results, the following compounds were selected
216 for experimental evaluation: methocarbamol, pantoprazole, 5-azacytidine, pyridoxal 5'-
217 phosphate, sulfamethizole vetranal, suprofen, sitaxentan, cytarabine, (e)-5,5'-(diazene-1,2-
218 diyl)bi, ticarcillin, nilutamide, adenosine, thymidine, tolbutamide, L-Histidine, sulfadiazin
219 vetranal and sulfamethoxazole. The selection criteria involved the number of favorable
220 interactions with polar residues in the MnaA active site, the absence of ligand polar groups
221 lacking interactions with the receptor and a reasonable match in the occupied volume as
222 compared to the substrate pose.
223

224 Experimental Screening of Ligand Candidates
225

226 A rapid assay for screening of the ligand candidates was set up using a DSF assay.
227 Initially, the enzyme melting curve was characterized in the apo state (unbound) as well as
228 bound to UDP, UDP-N-Acetylglucosamine and UDP + UDP-N-acetylglucosamine together. As
229 indicated in Figure 1, the melting temperatures (T_M) for the apo MnaA and for the enzyme
230 bound to UDP do not change significantly (54.4 and 55.2°C, respectively), suggesting that (i)
231 the enzyme binds very weakly to UDP in the absence of the substrate or (ii) the enzyme could
232 be pre-loaded with UDP after bacterial expression [13]. When bound to UDP-GlcNAc, in the
233 other hand, an important shift in the melting temperature was observed, as shown in Figure
234 1, with a T_M of 58.2°C. Interestingly, when both UDP and UDP-N-acetylglucosamine were
235 incubated with MnaA, the observed T_m was 58.7°C, very close to the T_m observed for UDP-N-
236 acetylglucosamine alone.

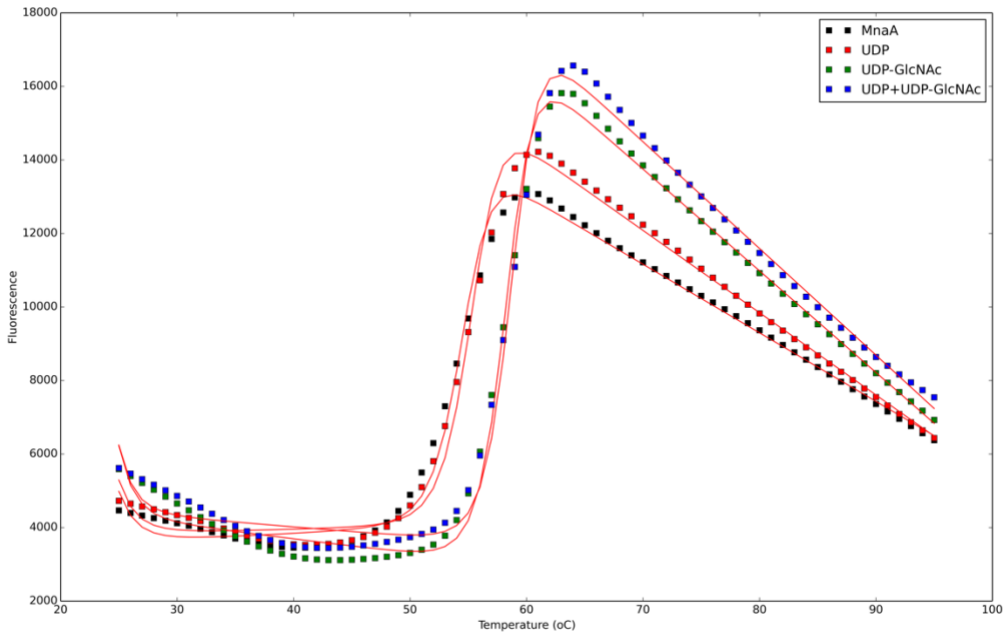

237

238 *Figure 1. Melting curves for unbound (apo) MnaA (black squares) and in complex with UDP (red squares), UDP-GlcNAc (green*
239 *squares) and UDP and UDP-GlcNAc simultaneously (blue squares). The red lines indicate the fit of the experimental data to*
240 *equations (1)-(3).*

241

242 This preliminary result indicated that, even the enzyme substrate, binds with a
243 relatively small change in the T_m, of about 4 degrees. So, in order to identify potential MnaA
244 binders, we searched for ligands that resulted in a T_m change of at least 2 degrees in a DSF
245 screening experiment. From the 17 initially purchased compounds, nine showed a T_M shift of
246 2 degrees or higher and were selected for further experimental evaluation. The ligand
247 candidates initially tagged as potential hits were methocarbamol, pantoprazole,
248 sulfamethiazole, suprofen, cytarabine, olsalazine, ticarcillin, nilutamide and sulfadiazine,
249 while sulfamethoxazole, tolbutamide, histidine, thymidine, pyridoxal 5'-phosphate were
250 discarded as potential ligands. 5-azacytidine revealed fluorescence signal in the absence of
251 protein and was removed from our analysis.

252

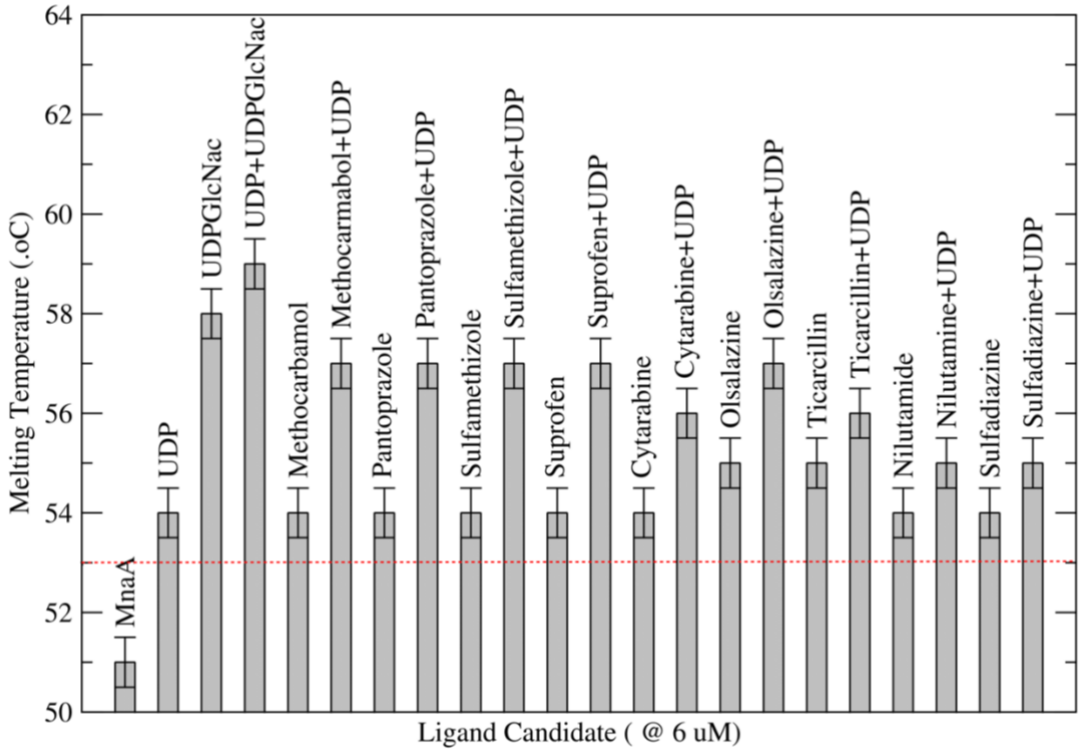

253

254 *Figure 2. Initial hits in the experimental ligand screening. SaMnaA (2μM) and the ligands identified in the virtual screening*
255 *(6μM) were preliminary tested for their binding properties using the DSF assay. A thermal shift of 2 degrees (red line) was*
256 *considered an indication of binding. In all cases, the incubation of the tested ligand with UDP increased the observed T_M.*

257

258 For a further exploration of the binding potential of the selected compounds,
259 quantitative DSF assay was setup, as previously described by Bai and coworkers [27], where
260 the change in T_M is monitored as a function of the ligand concentration. First, a positive
261 control experiment was set up, using MnaA substrate, UDP-GlcNac. The analysis of the
262 melting curves over a concentration range of 0 - 2,000 μM revealed a clear right-shift in the
263 melting temperature (T_m) for an increasing ligand concentration, as shown in Figure 3.
264 According to the global fitting of the data, measured in two independent replicates, at
265 T_m=54°C, a K_U of 1.08 was achieved with a K_D of 33 μM. At T_m=56°C, a K_U of 3.22 with a K_D of
266 31 μM were observed. Here, K_U is an equilibrium constant between the unfolded and folded
267 enzyme. So, a KU of 1 gives equal concentrations of folded and unfolded species. Interestingly,
268 the K_M for UDP-GlcNAc measured for SaMnaA was reported to be 411 ± 57μM according to
269 Mann and coworkers [13]. Clearly, the differences can be due to the assumptions of an
270 equilibrium interaction rather than a kinetic (enzymatic) model. In line with this observation,
271 a plot of $\ln K$ as function of $1/T$ does not show a typical linear dependency expected for the
272 van't Hoff relationship, indicating that the enthalpy may not be temperature independent.
273 This could be related to the change in enzyme activity over the temperature range, resulting
274 in this non-linear relationship.

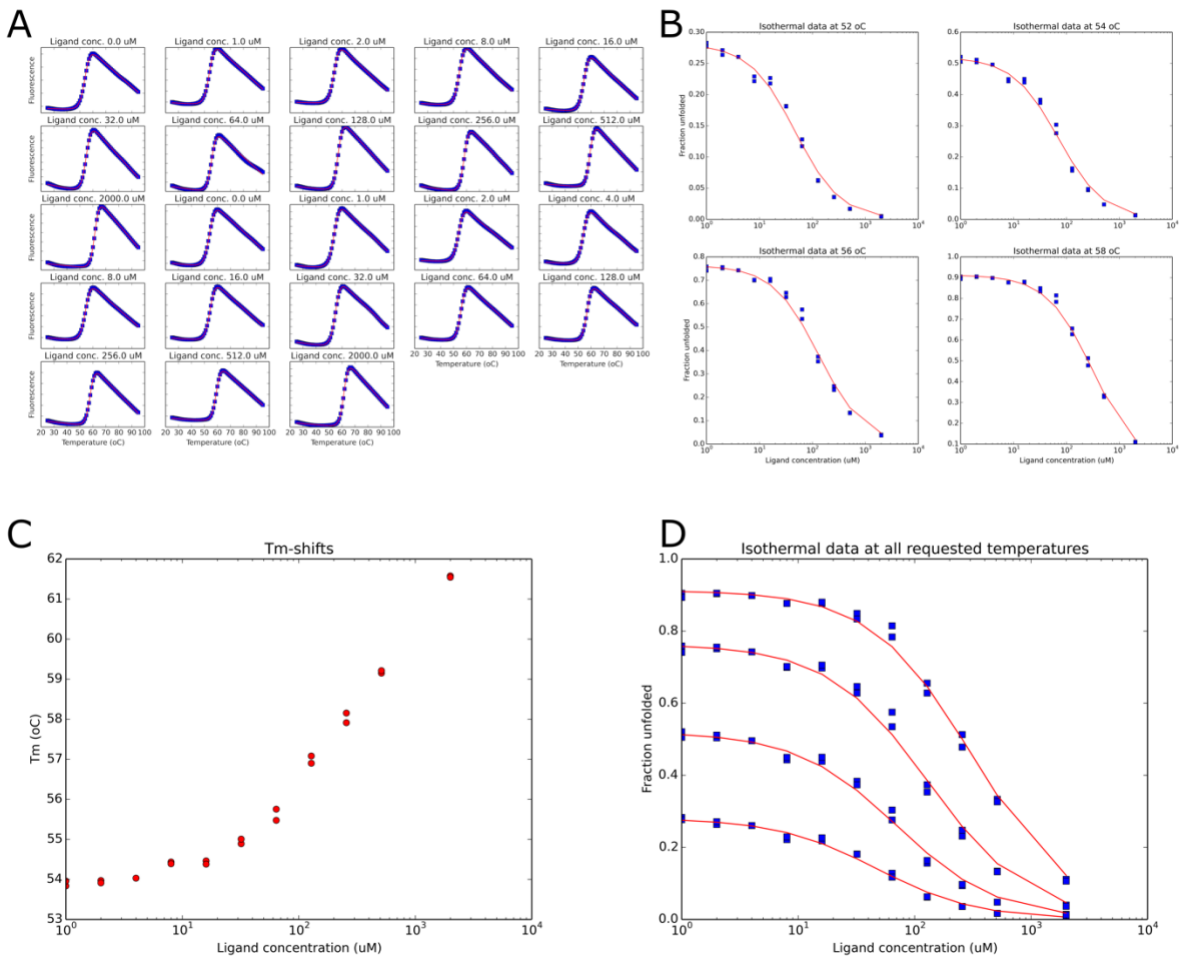

Figure 3. Isothermal analysis of UDP-GlcNAc binding to SaMnaA based on DSF data. (A) Thermal denaturation fluorescence data and fitting curve (red lines) for different ligand concentrations. (B) Fraction of unfolded protein as a function of UDP-GlcNac at different temperatures. (C) Shifts observed in the melting temperature T_M as a function of ligand concentration. (D) Overlay of the data shown in panel (B) of fraction of unfolded protein as a function of ligand concentration. In all cases, the red lines show the best fit obtained from the models shown in equations (1) to (10).

For most of the ligands selected in the initial screen, a clear T_M shift as a function of the ligand concentration could not be observed. Instead, a constant Tm was observed as a function of the ligand concentration, with a sharp increase in fluorescence in higher concentrations. This sharp increase in fluorescence can indicate some interaction between the ligand and fluorescent probe, for example.

For ticarcillin, however, the melting curves were measured in two replicates over a concentration range of 0-1,300 μM, limited by the ligand solubility, and at T_M=54°C a K_U of

289 1.08 was observed with a K_D of 421 μM (Figure 4). For ticarcillin, in contrast to what was

290 observed for UDP-GlcNAc, a linear relationship was observed for $\ln K$ as a function of $1/T$.

291

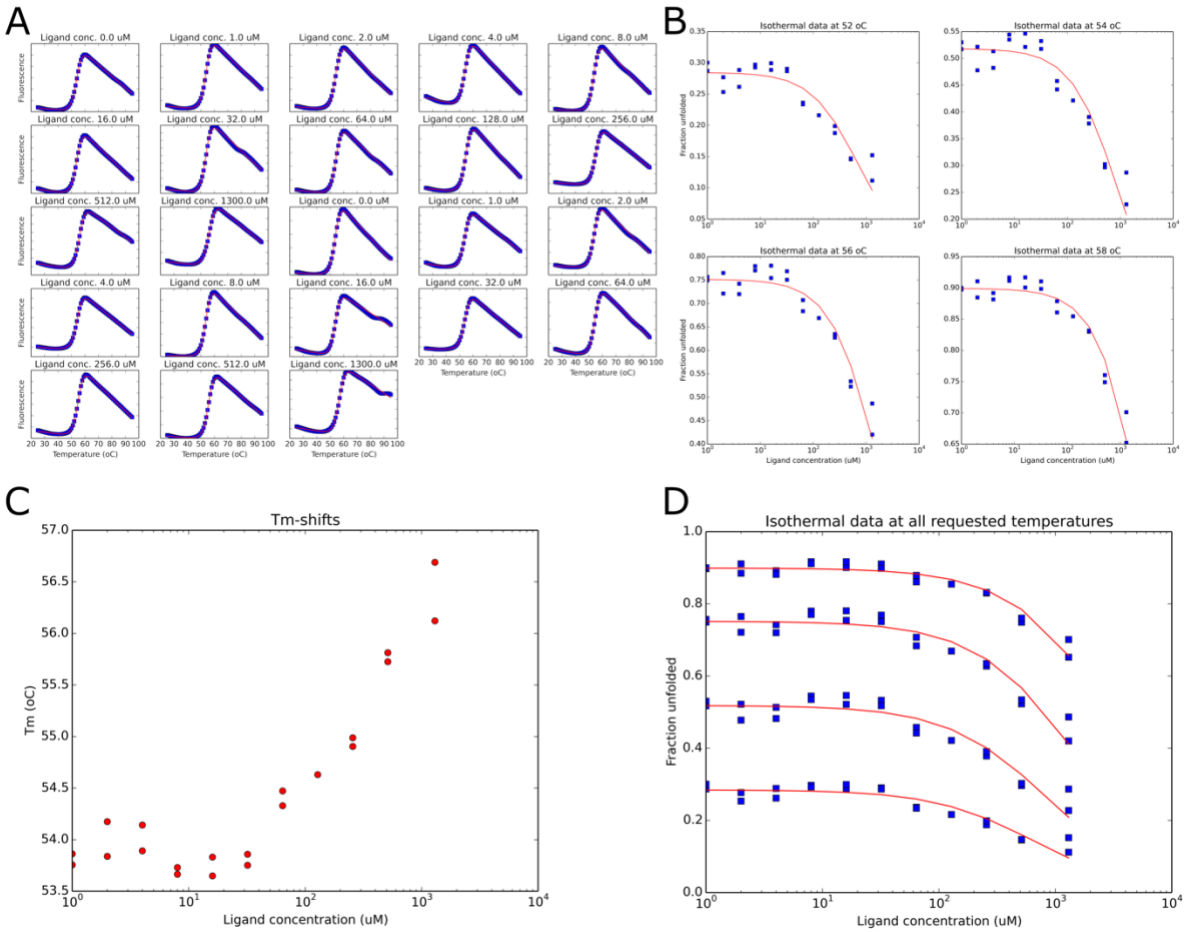

292

293 *Figure 4. Isothermal analysis of ticarcillin binding to SaMnaA based on DSF data. (A) Thermal denaturation fluorescence data*
294 *and fitting curve (red lines) for different ligand concentrations. (B) Fraction of unfolded protein as a function of ticarcillin at*
295 *different temperatures. (C) Shifts observed in the melting temperature T_M as a function of ligand concentration. (D) Overlay*
296 *of the data shown in panel (B) of fraction of unfolded protein as a function of ligand concentration. In all cases, the red lines*
297 *show the best fit obtained from the models shown in equations (1) to (10).*

298

299 The quantitative DSF data indicates that ticarcillin is a weak MnaA binder with a K_D in

300 the range of 400 μM, in our experimental conditions, what is about thirteen times greater

301 than the K_D measured for the substrate UDP-GlcNAc in our conditions. Although the

302 quantitative DSF approach does not measure the binding constant in an equilibrium situation,

303 previous data have shown that binding affinities agree very closely to the binding affinities

determined by other experimental approaches, such as Isothermal titration calorimetry (ITC) [27].

Molecular Dynamics Simulation of the SaMnaA-Ticarcillin Complex

The docked pose from ticarcillin bound to SaMnaA was used to generate the initial coordinates of the solvated complex for an equilibrium MD simulation. The obtained 600 ns trajectory was used for a cluster analysis in CPPTRAJ [36] and also in UCSF Chimera. In both cases, two major cluster were identified with minor differences among them. Figure 5 show the ligand bound to the SaMnaA, as observed in the most populated cluster in the MD simulation.

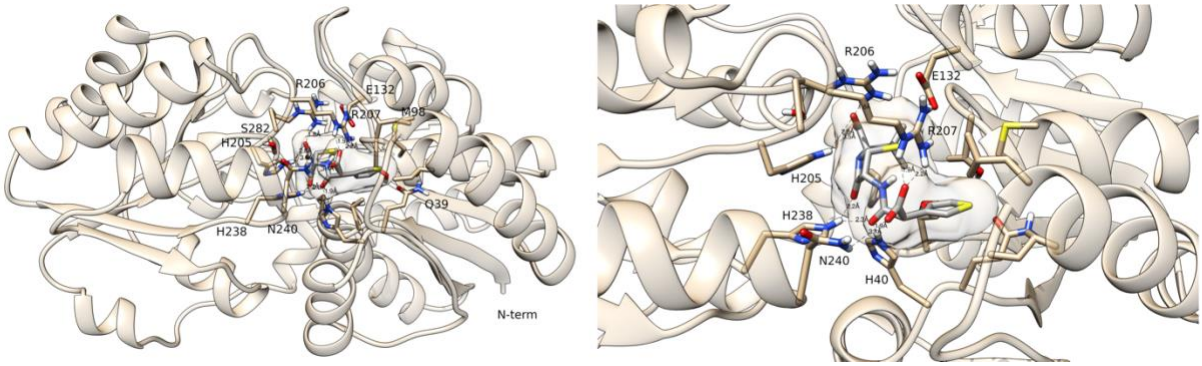

Figure 5. Representative frame of the most populated cluster during the MD simulation of the SaMnaA-ticarcillin complex. Solvent and non-polar hydrogen atoms were omitted for clarity. Ticarcillin is shown in gray sticks.

As shown in Figure 5, several polar residues interact with ticarcillin in the binding site, contributing to its binding affinity. Most importantly, H40, N240, H238, H205, R207 and R206 directly Interact with ticarcillin carboxylate groups as well as with carbonyl oxygen. As previously described, it is interesting to note that many positively charged residues surround the binding site, what would be expected for an enzyme that binding phosphorylated

substrates [16]. That said, ticarcillin seems to be a reasonable binder, given its total negative charge.

The individual contributions of each polar residue in the vicinity of the catalytic cleft were computed with `AmberEnergy++` and is shown in Figure 6 below. As evidenced in the left panel, the charged arginine residues have the largest contribution to the binding energy, with about -130 kcal/mol per residue, while the entire interaction energy between ticarcillin and the environment (MnaA and explicit solvent) sums about -450 kcal/mol (Figure 6, right panel). This finding is also in line with our previous analysis that showed that R206, R207 and K239 were the residues with largest contribution to UDP-GlcNac binding to MnaA [16]. Here, K239 contributes to about -50 kcal/mol to the ticarcillin binding energy.

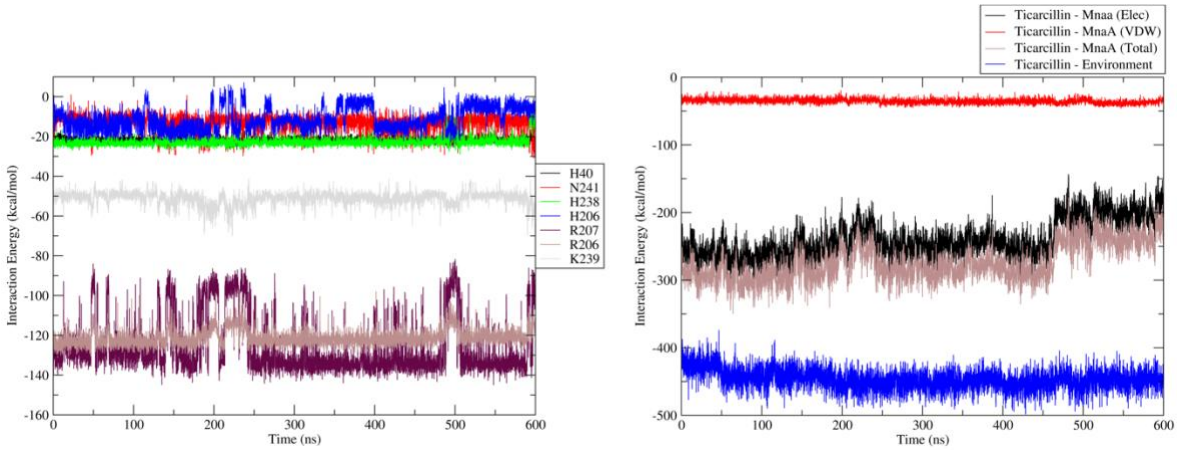

Figure 6. Interaction energies among ticarcillin and MnaA. (left) Decomposition analysis of the individual contributions to the binding energy for the polar residues in the vicinity of the active site. (right) Interaction energies computed for ticarcillin and the entire protein, as well as its electrostatic and van der Waals terms. The blue line shows the interaction energy of the ligand (ticarcillin) with the environment, i.e., protein and the explicit solvent.

Additional analysis of the interaction energy with MMPBSA.py [37] revealed an interaction energy of -47 ± 6 kcal/mol, using a Generalized Born (GB) model from Hawkins, Cramer and Truhlar [38]. In line with the previous analysis, ticarcillin binding to SaMnaA has a van der Waals contribution of -35 ± 4 kcal/mol, while the electrostatic contributions sum -

346 239 ± 28 kcal/mol. The GB correction for the (implicit) solvent adds +232 ± 24 kcal/mol,
347 resulting in a final binding energy if -47 kcal/mol.
348

349 Discussion

350
351

352 The limited number of molecular targets/pathways explored by existing antibiotics is
353 worrying [14]. The resistance problem is even more severe for some pathogens where high
354 resistance rates are observed. The data reported to the National Healthcare Safety Network
355 2015-2017 indicated, for example, that 48.4% of the *S. aureus* isolates from device-associated
356 healthcare associate infections in acute-care hospitals were found to be resistant to
357 methicillin (MRSA) [39]. 82.1% of the *Enterococcus faecium* isolates were found to be
358 vancomycin resistant and 43% of *Acinetobacter spp* were found to be resistant to multidrug
359 resistant [39]. These alarming trends highlight the need for new antibiotic targets and for the
360 basic and translational research on their mechanisms.

361 Here we described the structure-based identification of ticarcillin as a weak MnaA
362 binder. According to the docking model and to the binding mode observed in the MD
363 simulations, ticarcillin binds to the substrate pocket, putatively acting as a competitive
364 inhibitor, although this proposal still awaits for further experimental validation. This finding
365 has at least two interesting implications. The first implication is the usage of ticarcillin as a
366 scaffold for the development and optimization of compounds aiming higher affinity to
367 SaMnaA. Those compounds can be useful as chemical probes to better understand the effects
368 of SaMnaA inhibition in *S. aureus* cultures. Since ticarcillin is a β-lactam antibiotic, there is no
369 sense in testing it since a reduction in cell proliferation is already expected to be observed.

370 The second implication is associated with ticarcillin mechanism of action.
371 Interestingly, this β-lactam is expected to reach serum concentrations of up to 124 μg/ml
372 after an intravenous injection of 1 g [40], what means serum levels even between 300 and
373 400 μM. So, at these concentrations, MnaA could be expected to be partially bound to
374 ticarcillin. This off-target interaction for ticarcillin could explain, at least partially, the good
375 activity of ticarcillin on the Gram-negative bacteria *Pseudomonas aeruginosa*. *P. aeruginosa*
376 has a UDP-N-Acetylglucosamine 2-epimerase that shares about 51% in sequence identity with
377 *S. aureus* MnaA. The same is true for species of the *Acinetobacter* genus. Thus, it is tempting
378 to speculate that the MnaA inhibition may be associated to the ticarcillin activity on Gram-
379 negative bacteria. In line with this observation, it is interesting to note that the activity on
380 Gram-negative bacteria is only achieved at high concentrations [40], again suggesting a low-
381 affinity interaction with the target.
382 If this hypothesis is correct, is it possible to anticipate other pathogens that could be
383 susceptible to ticarcillin? According to a sequence comparison in BLAST [41], other UDP-N-
384 acetylglucosamine 2-epimerases are close orthologues of *S. aureus* MnaA, including a
385 *Mycoplasma* epimerase. Since *Mycoplasma* species are usually unresponsive to beta-lactams,
386 it may be a feasible experimental model to assess whether the UDP-N-acetylglucosamine can
387 inhibit the growth and, maybe, indicate a new therapeutic indication for ticarcillin. Although
388 this experiment is not accessible to us, we foresee very promising consequences of the
389 findings reported here.
390

391 # Acknowledgements
392

The authors thank Maria A. M. Santos, Lívia R. M. Margarido, Josimar Sartori and João F. Possatto, for their technical assistance. We also thank Fundação de Amparo à Pesquisa do Estado de São Paulo – FAPESP, for the financial support via grants 2020/03983-9, 2017/18173-0, 2015/26722-8, and 2015/13684-0; and the Conselho Nacional de Desenvolvimento Científico e Tecnológico – CNPq via grant 303165/2018-9. This study was also financed in part by the Coordenação de Aperfeiçoamento de Pessoal de Nível Superior – Brazil (CAPES) – Finance Code 001.

Author contributions

ASN wrote the original draft and supervised and administrated the project. ASN and ECA involved in the hypothesis generation, definition of the methodology, data acquisition and analysis. The final manuscript was revised by ASN and ECA.

Data accessibility

The data generated in this study are available from our group's GitHub account at https://github.com/alessandronascimento/LabData/tree/main/MnaA-Ticarcillin.

412 # References

413

414 1 CDC (2013) Antibiotic resistance threats in the USA. .

415 2 Weiner LM, Webb AK, Limbago B, Dudeck MA, Patel J, Kallen AJ, Edwards JR & Sievert DM

416 (2016) Antimicrobial-Resistant Pathogens Associated With Healthcare-Associated

417 Infections: Summary of Data Reported to the National Healthcare Safety Network at

418 the Centers for Disease Control and Prevention, 2011–2014. *Infect Control Hosp*

419 *Epidemiol* **37**, 1288–1301.

420 3 Sievert DM, Ricks P, Edwards JR, Schneider A, Patel J, Srinivasan A, Kallen A, Limbago B &

421 Fridkin S (2013) Antimicrobial-Resistant Pathogens Associated With Healthcare-

422 Associated Infections: Summary of Data Reported to the National Healthcare Safety

423 Network at the Centers for Disease Control and Prevention, 2019–2010. *Infect Control*

424 *Hosp Epidemiol* **34**, 1–14.

425 4 World Health Organization (2017) *[No Title]* Geneva.

426 5 Kelly R & Davies SC (2017) Tackling antimicrobial resistance globally. *Med J Aust* **207**, 371-

427 373.e1.

428 6 Thorpe KE, Joski P & Johnston KJ (2018) Antibiotic-resistant infection treatment costs have

429 doubled since 2002, now exceeding $2 billion annually. *Health Aff* **37**, 662–669.

430 7 Suginaka H, Blumberg PM & Strominger JL (1972) Multiple Penicillin-binding Components

431 in Bacillus subtilis, Bacillus cereus, Staphylococcus aureus, and Escherichia coli. *J Biol*

432 *Chem* **247**, 5279–5288.

433 8 Brown S, Santa Maria JP & Walker S (2013) Wall Teichoic Acids of Gram-Positive Bacteria.

434 *Annu Rev Microbiol* **67**, 313–336.

435 9 Brown S, Xia G, Luhachack LG, Campbell J, Meredith TC, Chen C, Winstel V, Gekeler C,

436 Irazoqui JE, Peschel a. & Walker S (2012) Methicillin resistance in Staphylococcus

437 aureus requires glycosylated wall teichoic acids. *Proc Natl Acad Sci* **109**.

438 10 Winstel V, Xia G & Peschel A (2014) Pathways and roles of wall teichoic acid glycosylation

439 in Staphylococcus aureus. *Int J Med Microbiol* **304**, 215–221.

440 11 Lee SH, Wang H, Labroli M, Koseoglu S, Zuck P, Mayhood T, Gill C, Mann P, Sher X, Ha S,

441 Yang S-W, Mandal M, Yang C, Liang L, Tan Z, Tawa P, Hou Y, Kuvelkar R, DeVito K, Wen

442 X, Xiao J, Batchlett M, Balibar CJ, Liu J, Xiao J, Murgolo N, Garlisi CG, Sheth PR, Flattery

443 A, Su J, Tan C & Roemer T (2016) TarO-specific inhibitors of wall teichoic acid

444 biosynthesis restore β-lactam efficacy against methicillin-resistant staphylococci. *Sci*

445 *Transl Med* **8**, 329ra32.

446 12 Hou Y, Mayhood T, Sheth P, Tan CM, Labroli M, Su J, Wyss DF, Roemer T & McCoy MA

447 (2016) NMR Binding and Functional Assays for Detecting Inhibitors of S. aureus MnaA. *J*

448 *Biomol Screen*.

449 13 Mann PA, Müller A, Wolff KA, Fischmann T, Wang H, Reed P, Hou Y, Li W, Müller CE, Xiao

450 J, Murgolo N, Sher X, Mayhood T, Sheth PR, Mirza A, Labroli M, Xiao L, McCoy M, Gill

451 CJ, Pinho MG, Schneider T & Roemer T (2016) Chemical Genetic Analysis and Functional

452 Characterization of Staphylococcal Wall Teichoic Acid 2-Epimerases Reveals

453 Unconventional Antibiotic Drug Targets. *PLOS Pathog* **12**, e1005585.

454 14 Walsh CT & Wencewicz T a (2013) Prospects for new antibiotics: a molecule-centered

455 perspective. *J Antibiot (Tokyo)* **67**, 7–22.

456 15 Farha MA & Brown ED (2019) Drug repurposing for antimicrobial discovery. *Nat*

457 *Microbiol*, 1.

458 16 de Azevedo EC & Nascimento AS (2019) Energy landscape of the domain movement in

459 Staphylococcus aureus UDP-N-acetylglucosamine 2-epimerase. *J Struct Biol*, 0–1.

460 17 Anandakrishnan R, Aguilar B & Onufriev A V (2012) H++ 3.0: Automating pK prediction

461 and the preparation of biomolecular structures for atomistic molecular modeling and
462 simulations. *Nucleic Acids Res* **40**, W537-41.
463 18 Maier JA, Martinez C, Kasavajhala K, Wickstrom L, Hauser KE & Simmerling C (2015)
464 ff14SB: Improving the Accuracy of Protein Side Chain and Backbone Parameters from
465 ff99SB. *J Chem Theory Comput* **11**, 3696–3713.
466 19 Rassolov VA, Ratner MA, Pople JA, Redfern PC & Curtiss LA (2001) 6-31G* basis set for
467 third-row atoms. *J Comput Chem* **22**, 976–984.
468 20 Irwin JJ, Sterling T, Mysinger MM, Bolstad ES & Coleman RG (2012) ZINC: A Free Tool to
469 Discover Chemistry for Biology. *J Chem Inf Model* **52**, 1757–1768.
470 21 dos Santos Muniz H & Nascimento AS (2015) Ligand- and receptor-based docking with
471 LiBELa. *J Comput Aided Mol Des* **29**, 713–723.
472 22 Li L, Li C, Zhang Z & Alexov E (2013) On the Dielectric "Constant" of Proteins: Smooth
473 Dielectric Function for Macromolecular Modeling and Its Implementation in DelPhi. *J
474 Chem Theory Comput* **9**, 2126–2136.
475 23 Li L, Li C, Sarkar S, Zhang J, Witham S, Zhang Z, Wang L, Smith N, Petukh M & Alexov E
476 (2012) DelPhi: a comprehensive suite for DelPhi software and associated resources.
477 *BMC Biophys* **5**, 9.
478 24 Sartori GR & Nascimento AS (2019) Comparative Analysis of Electrostatic Models for
479 Ligand Docking. *Front Mol Biosci* **6**, 1–8.
480 25 Pettersen EF, Goddard TD, Huang CC, Couch GS, Greenblatt DM, Meng EC & Ferrin TE
481 (2004) UCSF Chimera?A visualization system for exploratory research and analysis. *J
482 Comput Chem* **25**, 1605–1612.
483 26 Camilo CM & Polikarpov I (2014) High-throughput cloning, expression and purification of
484 glycoside hydrolases using Ligation-Independent Cloning (LIC). *Protein Expr Purif* **99**,

485 35–42.

486 27 Bai N, Roder H, Dickson A & Karanicolas J (2019) Isothermal Analysis of ThermoFluor Data

487 can readily provide Quantitative Binding Affinities. *Sci Rep* **9**, 1–15.

488 28 Pucci F, Kwasigroch JM & Rooman M (2017) SCooP: an accurate and fast predictor of

489 protein stability curves as a function of temperature. *Bioinformatics*.

490 29 Wang JM, Wolf RM, Caldwell JW, Kollman PA & Case DA (2004) Development and testing

491 of a general amber force field. *J Comput Chem* **25**, 1157–1174.

492 30 Case DA, Cheatham TE, Darden T, Gohlke H, Luo R, Merz KM, Onufriev A, Simmerling C,

493 Wang B & Woods RJ (2005) The Amber biomolecular simulation programs. *J Comput*

494 *Chem* **26**, 1668–1688.

495 31 Salomon-Ferrer R, Case DA & Walker RC (2013) An overview of the Amber biomolecular

496 simulation package. *WIREs Comput Mol Sci* **3**, 198–210.

497 32 Salomon-Ferrer R, Götz AW, Poole D, Le Grand S & Walker RC (2013) Routine

498 Microsecond Molecular Dynamics Simulations with AMBER on GPUs. 2. Explicit Solvent

499 Particle Mesh Ewald. *J Chem Theory Comput* **9**, 3878–3888.

500 33 Le Grand S, Götz AW & Walker RC (2013) SPFP: Speed without compromise - A mixed

501 precision model for GPU accelerated molecular dynamics simulations. *Comput Phys*

502 *Commun* **184**, 374–380.

503 34 Nascimento AS (2018) AmberEnergy++.

504 *https://github.com/alessandronascimento/amberenergy*.

505 35 Humphrey W, Dalke A & Schulten K (1996) VMD: Visual molecular dynamics. *J Mol Graph*

506 **14**, 33–38.

507 36 Roe DR & Cheatham TE (2013) PTRAJ and CPPTRAJ: Software for processing and analysis

508 of molecular dynamics trajectory data. *J Chem Theory Comput* **9**, 3084–3095.

509 37 Miller BR, McGee TD, Swails JM, Homeyer N, Gohlke H & Roitberg AE (2012)
510 MMPBSA.py: An efficient program for end-state free energy calculations. *J Chem*
511 *Theory Comput* **8**, 3314–3321.
512 38 Hawkins GD, Cramer CJ & Truhlar DG (1996) Parametrized Models of Aqueous Free
513 Energies of Solvation Based on Pairwise Descreening of Solute Atomic Charges from a
514 Dielectric Medium. *J Phys Chem* **100**, 19824–19839.
515 39 Weiner-Lastinger LM, Abner S, Edwards JR, Kallen AJ, Karlsson M, Magill SS, Pollock D,
516 See I, Soe MM, Walters MS & Dudeck MA (2020) Antimicrobial-resistant pathogens
517 associated with adult healthcare-associated infections: Summary of data reported to
518 the National Healthcare Safety Network, 2015–2017. *Infect Control Hosp Epidemiol* **41**,
519 1–18.
520 40 Tavares W (2001) *Manual de Antibióticos e Quimioterápicos Antiinfecciosos*, 3rd ed.
521 Editora Atheneu, São Paulo.
522 41 Camacho C, Coulouris G, Avagyan V, Ma N, Papadopoulos J, Bealer K & Madden TL (2009)
523 BLAST+: Architecture and applications. *BMC Bioinformatics* **10**, 1–9.
524
525

526 # Figure Captions
527

528 **Figure 1**. Melting curves for unbound (apo) MnaA (black squares) and in complex with UDP
529 (red squares), UDP-GlcNAc (green squares) and UDP and UDP-GlcNAc simultaneously (blue
530 squares). The red lines indicate the fit of the experimental data to equations (1)-(3).
531

532 **Figure 2**. Initial hits in the experimental ligand screening. SaMnaA (2 μM) and the ligands
533 identified in the virtual screening (6 μM) were preliminary tested for their binding properties
534 using the DSF assay. A thermal shift of 2 degrees (red line) was considered an indication of
535 binding. In all cases, the incubation of the tested ligand with UDP increased the observed T_M.
536

537 **Figure 3**. Isothermal analysis of UDP-GlcNAc binding to SaMnaA based on DSF data. (A)
538 Thermal denaturation fluorescence data and fitting curve (red lines) for different ligand
539 concentrations. (B) Fraction of unfolded protein as a function of UDP-GlcNac at different
540 temperatures. (C) Shifts observed in the melting temperature T_M as a function of ligand
541 concentration. (D) Overlay of the data shown in panel (B) of fraction of unfolded protein as a
542 function of ligand concentration. In all cases, the red lines show the best fit obtained from the
543 models shown in equations (1) to (10).
544

545 **Figure 4**. Isothermal analysis of ticarcillin binding to SaMnaA based on DSF data. (A) Thermal
546 denaturation fluorescence data and fitting curve (red lines) for different ligand
547 concentrations. (B) Fraction of unfolded protein as a function of ticarcillin at different
548 temperatures. (C) Shifts observed in the melting temperature TM as a function of ligand
549 concentration. (D) Overlay of the data shown in panel (B) of fraction of unfolded protein as a

550 function of ligand concentration. In all cases, the red lines show the best fit obtained from the
551 models shown in equations (1) to (10).
552
553 **Figure 5**. Representative frame of the most populated cluster during the MD simulation of
554 the SaMnaA-ticarcillin complex. Solvent and non-polar hydrogen atoms were omitted for
555 clarity. Ticarcillin is shown in gray sticks.
556
557 **Figure 6**. Interaction energies among ticarcillin and MnaA. (left) Decomposition analysis of
558 the individual contributions to the binding energy for the polar residues in the vicinity of the
559 active site. (right) Interaction energies computed for ticarcillin and the entire protein, as well
560 as its electrostatic and van der Waals terms. The blue line shows the interaction energy of the
561 ligand (ticarcillin) with the environment, i.e., protein and the explicit solvent.
562

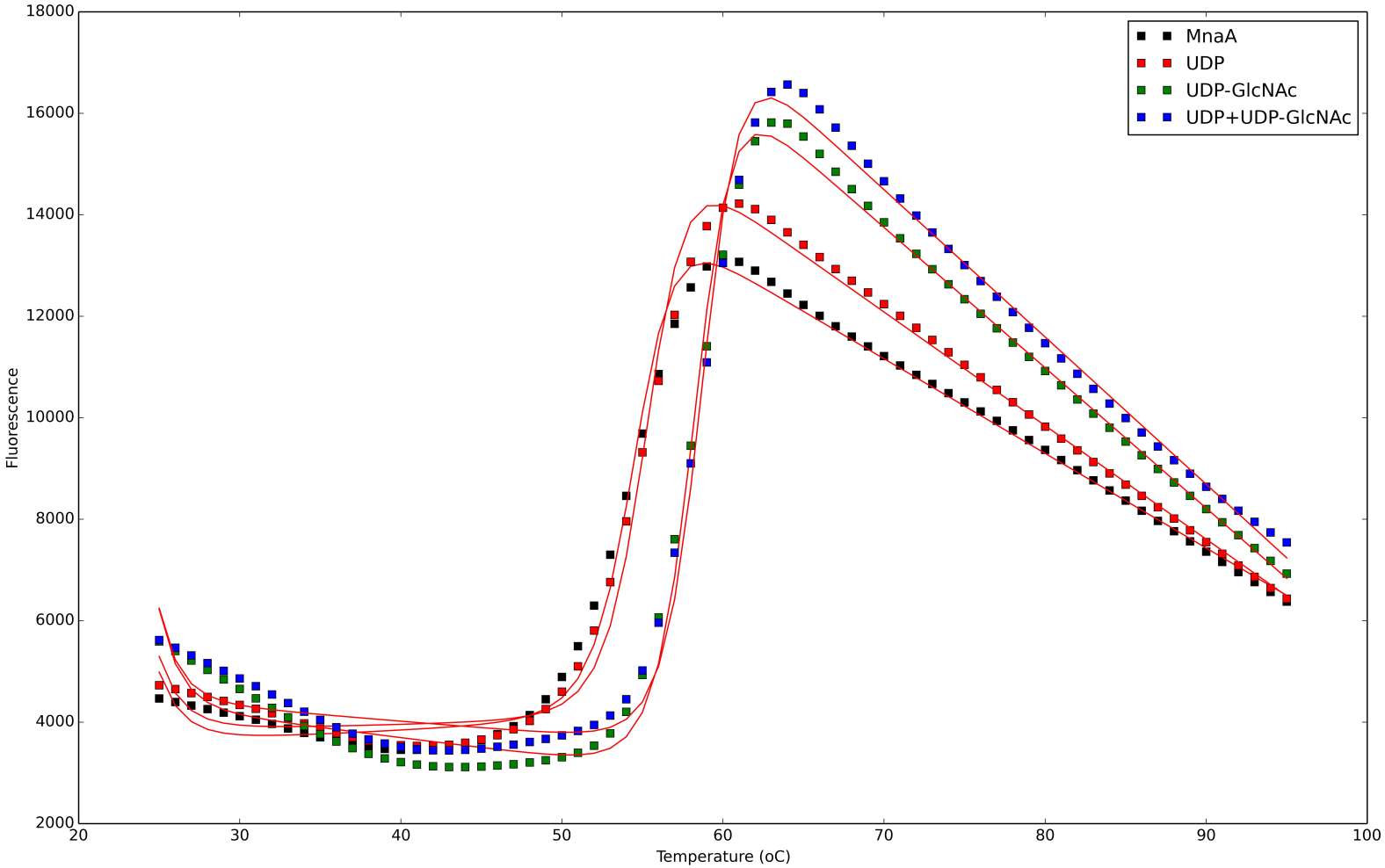
MnaA
UDP
UDP-GlcNAc
UDP+UDP-GlcNAc
Fluorescence
Temperature (oC)
18000
16000
14000
12000
10000
8000
6000
4000
2000
20
30
40
50
60
70
80
90
100

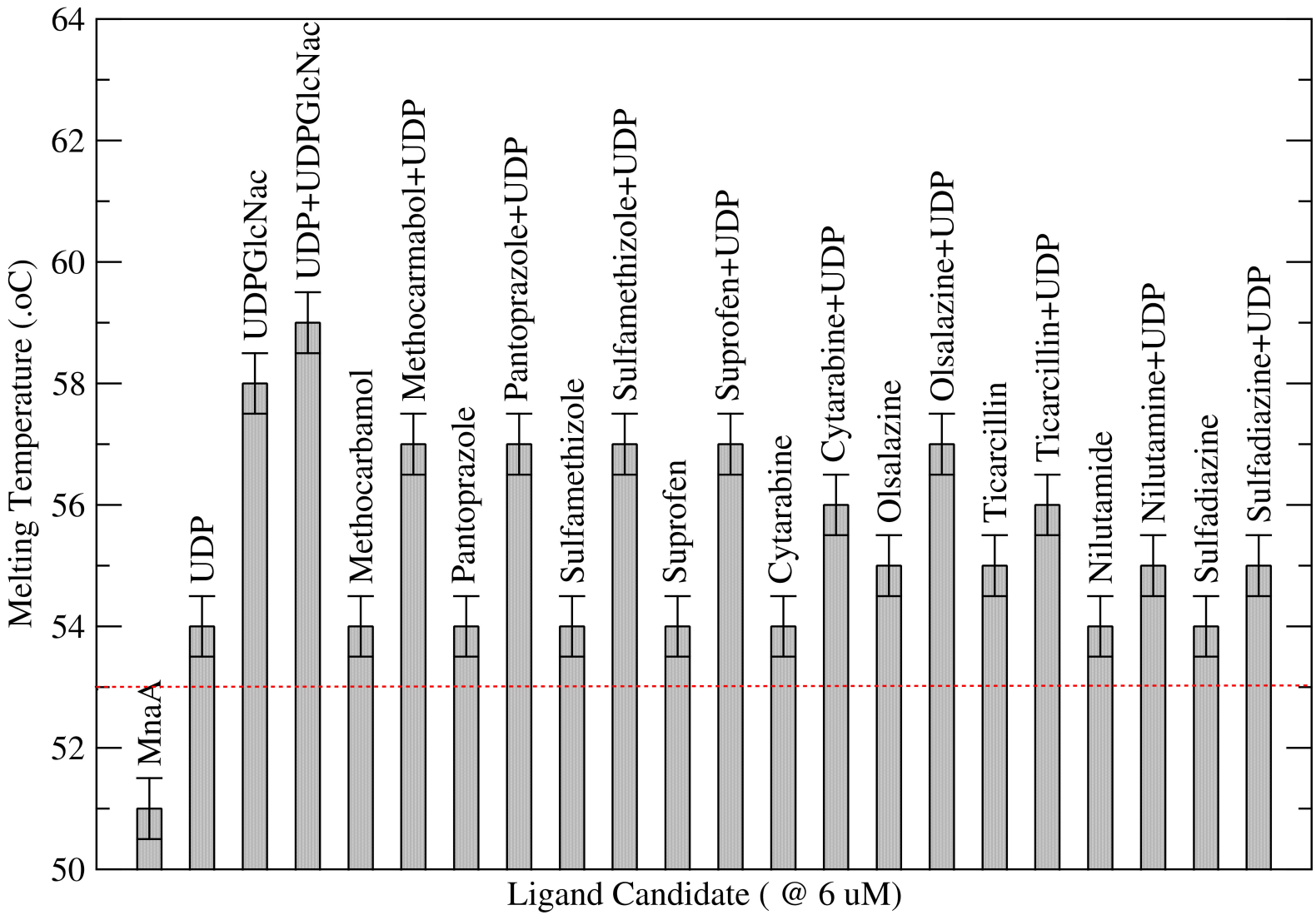
Melting Temperature (.oC)
64
62
60
58
56
54
52
50
MnaA
UDP
UDPGlcNac
UDP+UDPGlcNac
Methocarbamol
Methocarmabol+UDP
Pantoprazole
Pantoprazole+UDP
Sulfamethizole
Sulfamethizole+UDP
Suprofen
Suprofen+UDP
Cytarabine
Cytarabine+UDP
Olsalazine
Olsalazine+UDP
Ticarcillin
Ticarcillin+UDP
Nilutamide
Nilutamine+UDP
Sulfadiazine
Sulfadiazine+UDP
Ligand Candidate (@ 6 uM)

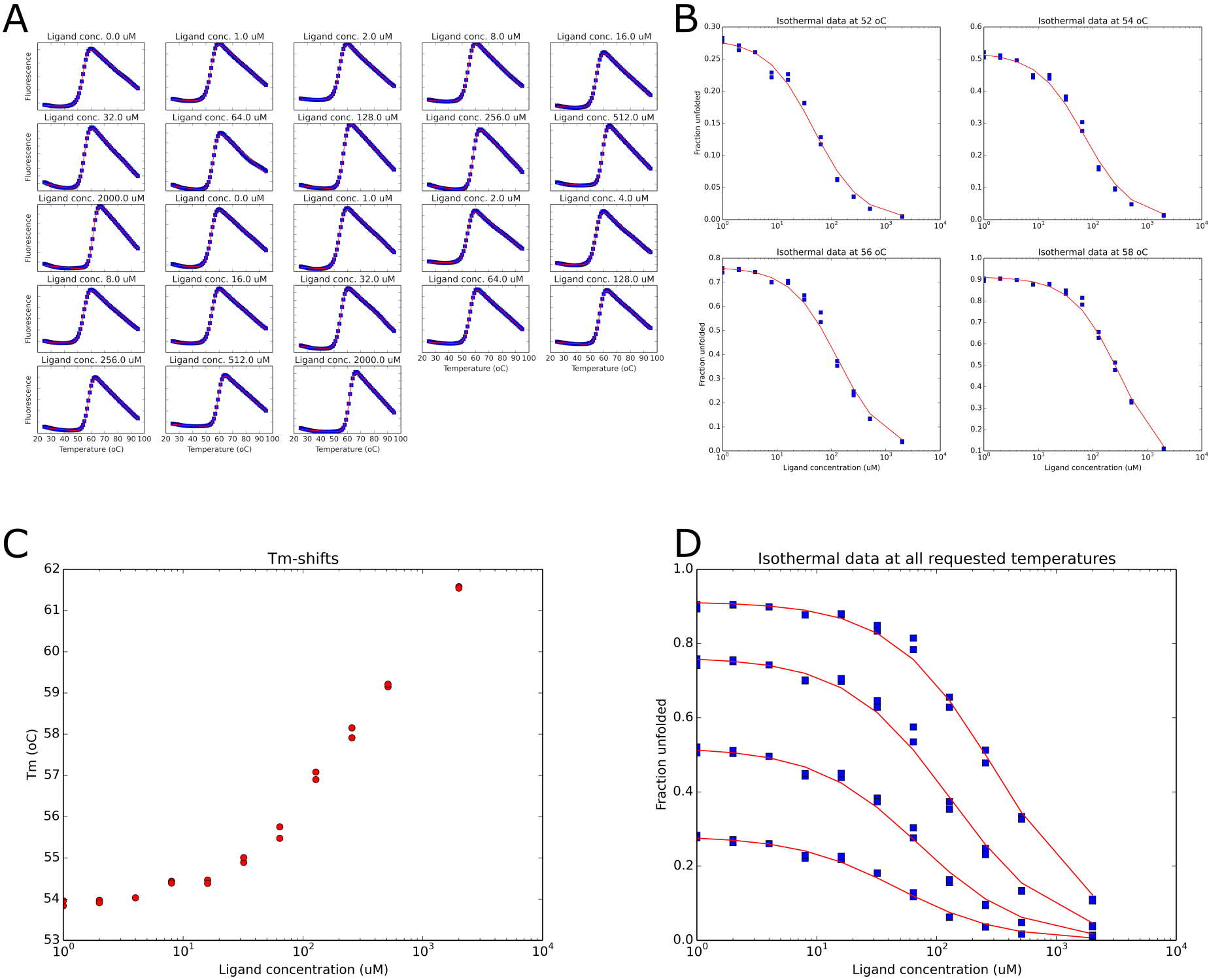
A
Ligand conc. 0.0 uM
Ligand conc. 1.0 uM
Ligand conc. 2.0 uM
Ligand conc. 8.0 uM
Ligand conc. 16.0 uM
Ligand conc. 32.0 uM
Ligand conc. 64.0 uM
Ligand conc. 128.0 uM
Ligand conc. 256.0 uM
Ligand conc. 512.0 uM
Ligand conc. 2000.0 uM
Ligand conc. 0.0 uM
Ligand conc. 1.0 uM
Ligand conc. 2.0 uM
Ligand conc. 4.0 uM
Ligand conc. 8.0 uM
Ligand conc. 16.0 uM
Ligand conc. 32.0 uM
Ligand conc. 64.0 uM
Ligand conc. 128.0 uM
Ligand conc. 256.0 uM
Ligand conc. 512.0 uM
Ligand conc. 2000.0 uM
Fluorescence
Temperature (oC)
B
Isothermal data at 52 oC
Isothermal data at 54 oC
Isothermal data at 56 oC
Isothermal data at 58 oC
Fraction unfolded
Ligand concentration (uM)
C
Tm-shifts
Tm (oC)
Ligand concentration (uM)
D
Isothermal data at all requested temperatures
Fraction unfolded
Ligand concentration (uM)

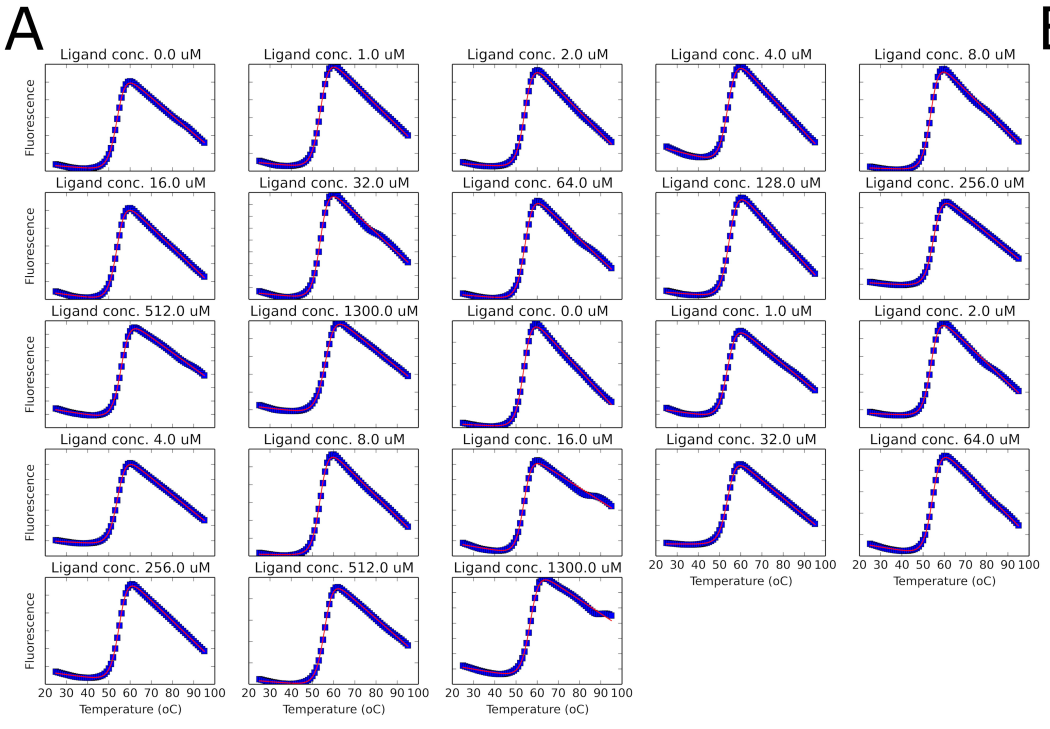
A
Ligand conc. 0.0 uM
Ligand conc. 1.0 uM
Ligand conc. 2.0 uM
Ligand conc. 4.0 uM
Ligand conc. 8.0 uM
Ligand conc. 16.0 uM
Ligand conc. 32.0 uM
Ligand conc. 64.0 uM
Ligand conc. 128.0 uM
Ligand conc. 256.0 uM
Ligand conc. 512.0 uM
Ligand conc. 1300.0 uM
Ligand conc. 0.0 uM
Ligand conc. 1.0 uM
Ligand conc. 2.0 uM
Ligand conc. 4.0 uM
Ligand conc. 8.0 uM
Ligand conc. 16.0 uM
Ligand conc. 32.0 uM
Ligand conc. 64.0 uM
Ligand conc. 256.0 uM
Ligand conc. 512.0 uM
Ligand conc. 1300.0 uM
Fluorescence
Temperature (oC)

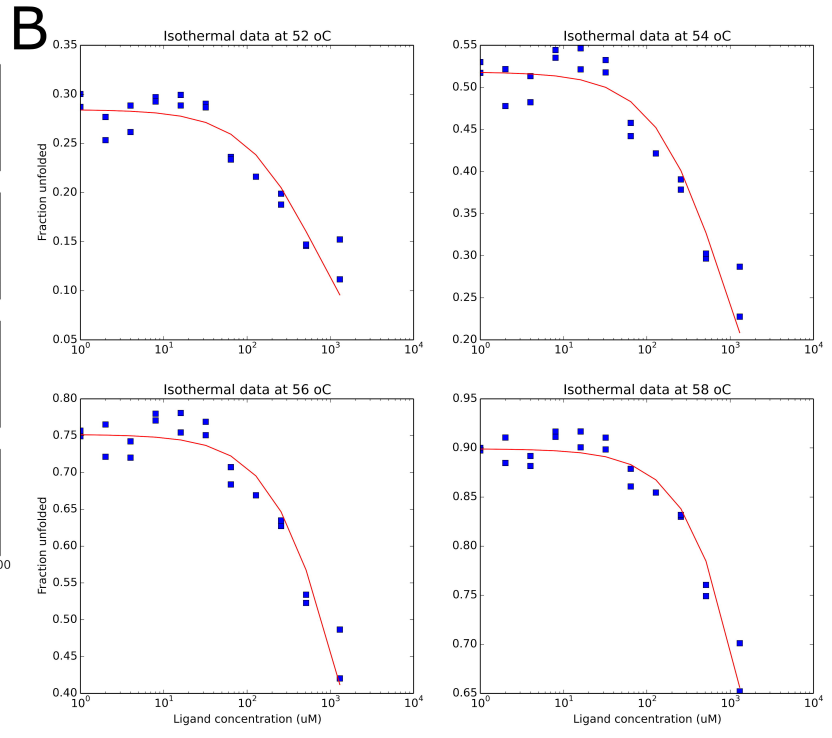
B
Isothermal data at 52 oC
Isothermal data at 54 oC
Isothermal data at 56 oC
Isothermal data at 58 oC
Fraction unfolded
Ligand concentration (uM)

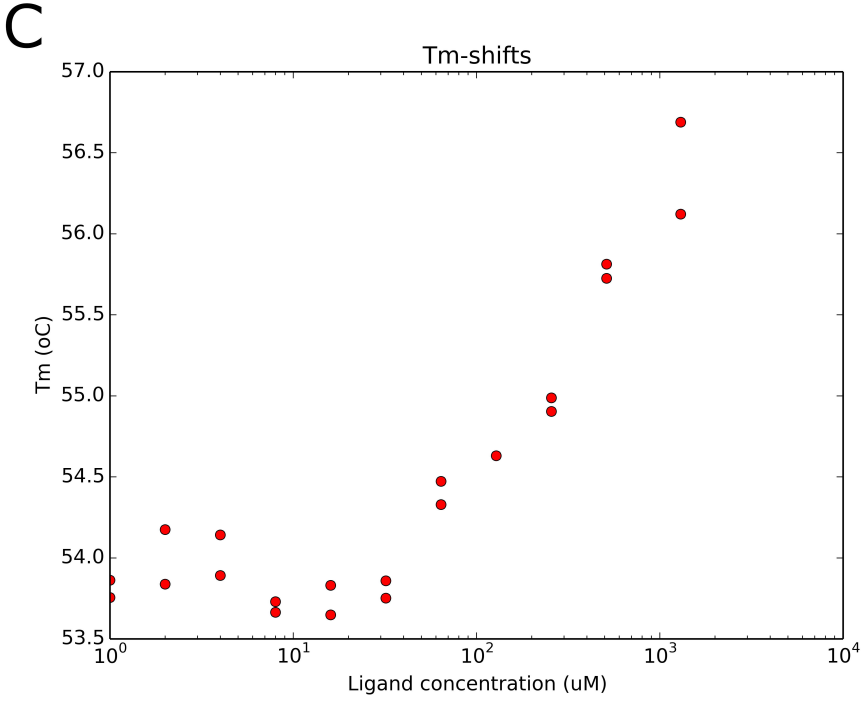
C
Tm-shifts
Tm (oC)
Ligand concentration (uM)

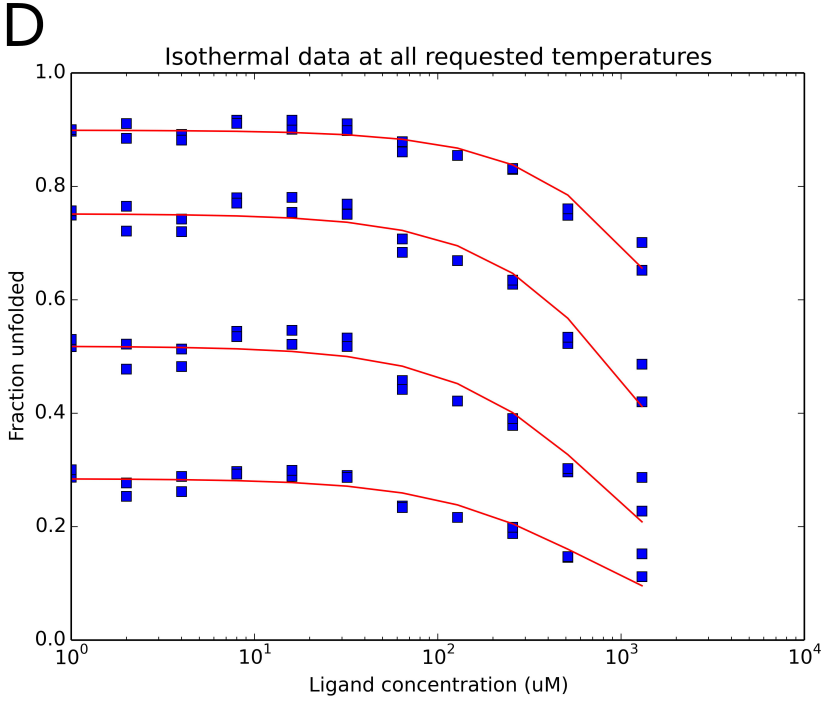
D
Isothermal data at all requested temperatures
Fraction unfolded
Ligand concentration (uM)

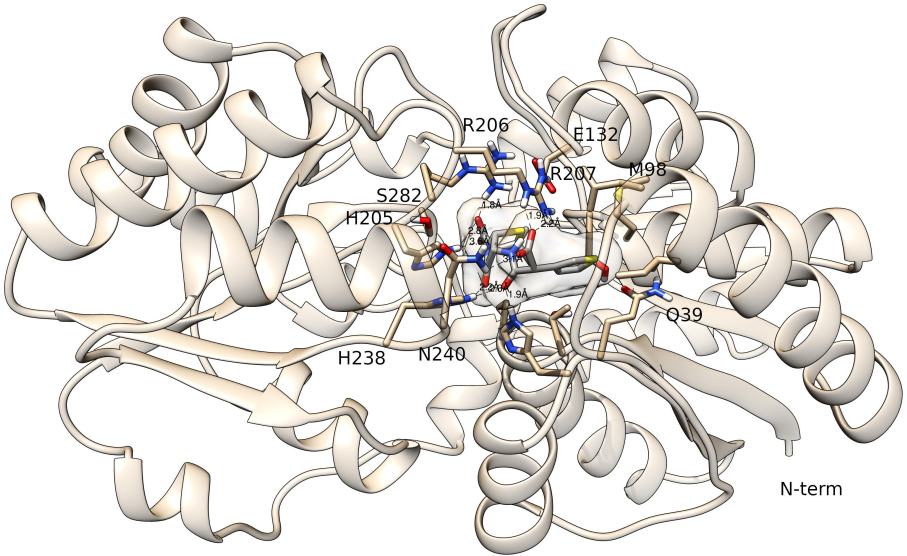
R206
E132
R207
M98
S282
H205
O39
H238
N240
N-term

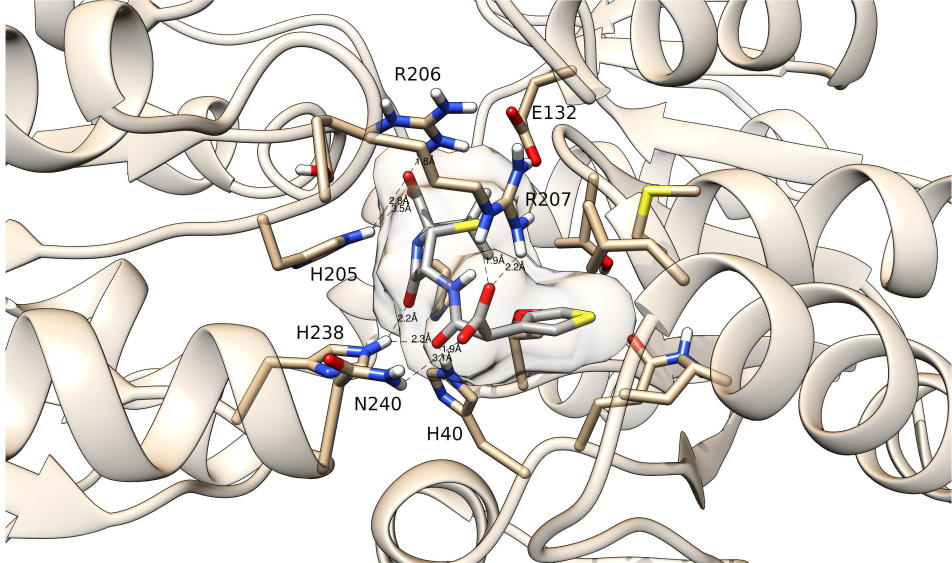
R206
E132
R207
H205
H238
N240
H40

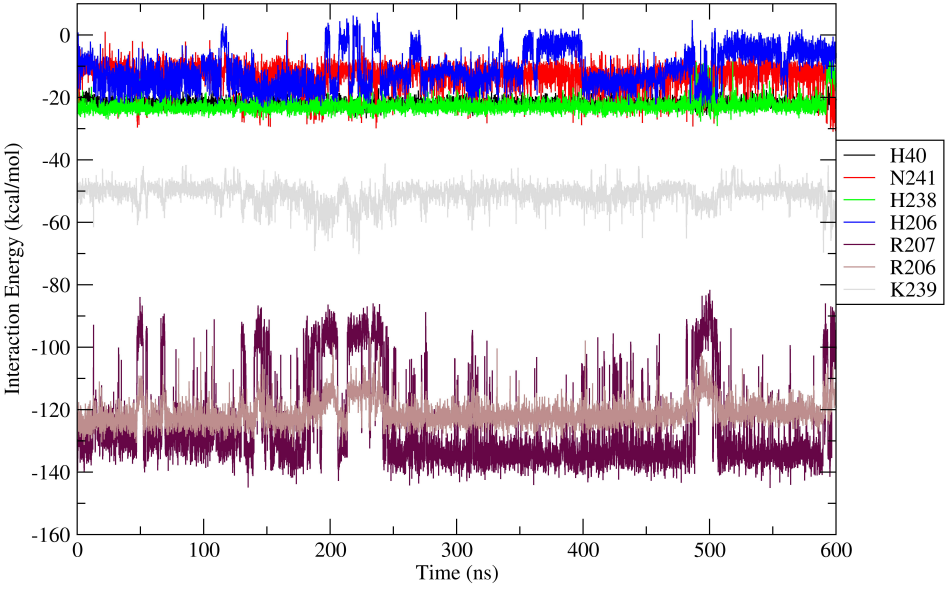
Interaction Energy (kcal/mol)
Time (ns)
0
-20
-40
-60
-80
-100
-120
-140
-160
0
100
200
300
400
500
600
H40
N241
H238
H206
R207
R206
K239

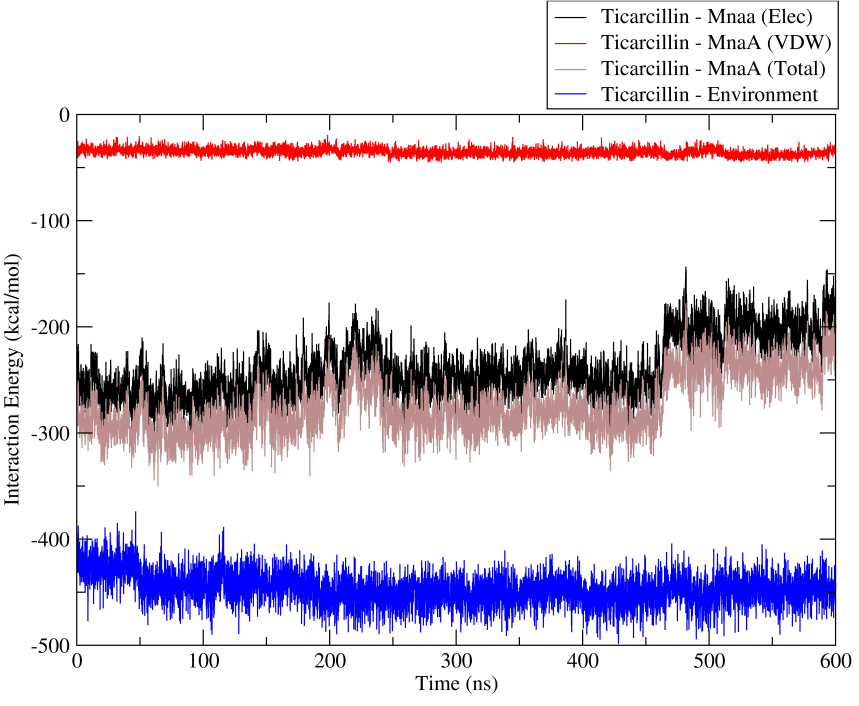
Ticarcillin - Mnaa (Elec)
Ticarcillin - MnaA (VDW)
Ticarcillin - MnaA (Total)
Ticarcillin - Environment
Interaction Energy (kcal/mol)
Time (ns)
0
-100
-200
-300
-400
-500
0
100
200
300
400
500
600